The Astrophysical Journal Letters, 737:L14 (5pp), 2011 August 10 doi:10.1088/2041-8205/737/1/L14

SOLID-STATE CO OXIDATION BY ATOMIC O: A ROUTE TO SOLID CO_2 SYNTHESIS IN DENSE MOLECULAR CLOUDS

U. Raut and R. A. Baragiola
Laboratory for Atomic and Surface Physics, University of Virginia, Thornton Hall B-114, Charlottesville, VA 22904, USA;
ur5n@virginia.edu, raul@virginia.edu
Received 2011 May 10; accepted 2011 July 2; published 2011 July 21

ABSTRACT

Investigations with infrared spectroscopy and microgravimetry show that CO_2 forms in small quantities during codeposition of CO and cooled O and O_2 into thin films at 20 K: $\sim 3 \times 10^{14}$ CO_2 cm^{-2} within a film containing 2.7×10^{17} CO cm^{-2}. The reason for the low CO_2 yield is that O atoms react preferentially with O to form O_2, and with O_2 to form ozone, which was not considered in previous studies with atomic beams. Heating a CO + O + O_2 film capped with a ~ 2.5 μm thick water ice layer to 80 K increased CO_2 by 30%, showing additional reactions between O and CO diffusing in the ice layer. Although the CO_2:CO $= 10^{-3}$ measured in our experiments is at least two orders of magnitude smaller than reported interstellar ratios, sputtering and differential desorption during transient heating events, e.g., by impacts of cosmic rays or stellar winds, can increase the ratio to observed values.

Key words: astrochemistry – infrared: ISM – ISM: abundances – ISM: molecules – methods: laboratory – molecular processes

Online-only material: color figure

1. INTRODUCTION

Understanding the origin of molecules in the interstellar medium (ISM) is a central problem in astrophysics whose solution requires laboratory investigations to complement observations. A particularly interesting and unresolved problem is the origin of carbon dioxide, which is abundant in the solid phase but not as interstellar gas. Condensed CO_2 has been detected in infrared absorbance spectra along multiple lines of sight in the ISM with abundances ranging from 10% to 30% relative to water ice (Boogert et al. 2004; Chiar et al. 2011).

The observation of condensed CO_2, in spite of its low abundance in the gas phase, suggests that it is formed on grains from the abundant parent molecule CO. Two mechanisms have been proposed for CO_2 formation, both requiring oxidation of CO by O atoms, which either accrete on the grain from the gas phase or are formed by dissociation of neighboring molecules in the ice, such as O_2 or H_2O, by radiation such as Lyα, cosmic rays, or stellar winds. The latter mechanism is not favored by laboratory studies (Gerakines & Moore 2001; Loeffler et al. 2005; Satorre et al. 2000; Watanabe & Kouchi 2002), which show that irradiation of solid CO by Lyα or fast ions produce CO_2:CO ratios that are much smaller than those observed in the ISM.

The exothermic reaction O + CO + M $\rightarrow$ CO_2 + M has a potential barrier of 17 kJ mol^{-1} (2000 K) in the gas phase (Slanger 1972). In the solid, there have been conflicting experiments with controversial results, partly because previous experiments could not control the internal excitation or kinetic energy of the O atoms. These studies irradiated CO mixed with N_2O (Fournier et al. 1979) or O_2 (Grim & D'Hendecourt 1986) with ultraviolet photons. The ice mixtures were diluted in an Ar matrix in both experiments. The O atoms that react with CO were generated via photodissociation of N_2O or O_2 and thus could be in translationally and electronically hot states (^1D, ^1S). More direct measurements have used O beams incident on condensed gases. In such experiments, Sethi et al. formed CO_2 between 70 and 140 K (Sethi & Smith 1975; Sharpe et al. 1988). The independence of their results on temperature suggests that there is a very small barrier, or none at all. More recently, Roser et al. codeposited CO on a Cu substrate at 5 K with ground state O atoms from a $\sim$50 W radio-frequency discharge and cooled to liquid nitrogen temperatures (Roser et al. 2001). A mass spectrometer detector did not show CO_2 in the desorbed flux when warming the film to 60 K. However, CO_2 was detected by the mass spectrometer, with a low signal-to-noise ratio, when the deposit was capped with a $\sim$100 ML ice layer and warmed to 160 K. They assumed that O + CO reactions occur in the ice pores during heating and derived an activation energy of 290 K. The model has many missing pieces or unknowns such as formation of O_2 and O_3, as well as migration rates for different species in the ice, and thus it is difficult to assess the reliability of the reported value. However, the activation energy is not inconsistent with the previous observations of CO_2 formation at 77 K (Sharpe et al. 1988). The lowering of the barrier in the solid is not unexpected. The mean distance between O–CO pairs in the solid is $\sim$0.2 nm, calculated from the minimum barrier in the gas phase (Braunstein & Duff 2000). Additional interactions with other species in the solid will strongly perturb the potential energy surfaces.

The question of the temperature required for CO_2 synthesis via CO oxidation by O in laboratory timescales has remained unanswered. Roser et al. did not detect CO_2 below 60 K (Roser et al. 2001), but this could have resulted from low sensitivity, since this temperature is close to 77 K, at which Sharpe et al. detected CO_2 using infrared spectroscopy (Sharpe et al. 1988). To resolve this apparent conflict or uncertainty, we undertook experiments condensing CO with O atoms at 20 K, but using more sensitive and quantitative detection methods. We combined infrared spectroscopy and microgravimetry to detect CO_2 in the condensate and obtained absolute numbers for the amounts of reactants and reaction products.

2. EXPERIMENTAL SETUP

Atomic oxygen was delivered to the gold substrate from a radio frequency (RF)-based Mantis MATS30 atom source

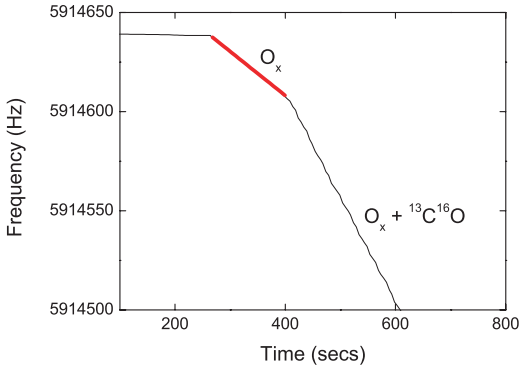

Figure 1. Change in frequency of the quartz crystal microbalance (QCM) during deposition of $^{13}C^{16}O$ and O_x at 20 K. The thick red line indicates deposition of O_x species from the atom source condensing at 0.22 Hz s^{-1}, equivalent to 1×10^{14} O atoms cm^{-2} s^{-1}. The deposition rate increases to 0.51 Hz s^{-1} as $^{13}C^{16}O$ is admitted into the chamber at $t = 400$ s due to the additional flux of 0.5×10^{14} ^{13}CO cm^{-2} s^{-1}. The O atom flux was directed at normal incidence to the QCM, while ^{13}CO was deposited at 60° incidence.

(A color version of this figure is available in the online journal.)

connected to the main chamber via a two-stage, differentially pumped beam line. The source was operated at 600 W, which partially dissociates O_2 gas to form an oxygen plasma. Deflection plates biased at 500 VDC removed the charged species in the plasma beam. The O_x neutrals (O and O_2; the absence of O_3 is discussed later) travel undeflected and undergo multiple collisions with a quartz thermalizer that is at a few hundred degrees Celsius. The beam then enters a Teflon-coated Al tube cooled to 40 K, acting as a second thermalizer, where the neutrals undergo additional collisions that lower their translational energy. The non-reactive Teflon coating inhibits recombination of the atomic oxygen flux (Mulcahy & Williams 1968). Such collisions should also remove electronic excited states O (^1D or ^1S), since they quench efficiently in gas phase collisions (Noxon 1970; Welge & Atkinson 1976). Thus, the beam striking the target is composed of ground state O and O_2 cooled to ~40 K. The atomic fraction of the beam is estimated at 40% ± 10%, typical for RF sources.

After passing another stage of differential pumping, neutral oxygen species entered the main target chamber at 10^{-10} Torr and deposited at normal incidence on top of the gold substrate of a quartz crystal microbalance (QCM) cooled to 20 K, whose resonant frequency changes proportionally to the areal mass of the deposit (Sack & Baragiola 1993). A typical response of the QCM during deposition is shown in Figure 1. The frequency of the microbalance decreases at a linear rate as O_x begins to condense on the QCM (Figure 1, red line). Typical deposition rates of the neutrals were ~0.2–0.25 Hz s^{-1}, equivalent to ~0.1 ML s^{-1} of O (1 monolayer (ML) is defined here as 10^{15} molecules cm^{-2}). Once an initial rate is established, isotopically labeled $^{13}C^{16}O$ (>98% isotopic purity) was deposited at 60° incidence through a microcapillary doser. The total deposition rate increased to 0.5–0.55 Hz s^{-1}, due to additional flux of ~0.06 ML s^{-1} of ^{13}CO. Close to the end of the film growth, the CO deposition was stopped, and the O_x deposition was continued briefly to compare with the initial deposition rate. The terminal O_x flux was usually within 2% of the initial O_x flux. We obtained uniformly mixed films of $^{13}C^{16}O$ and neutral O species. The film thickness depends on the relative proportion of the main constituents (CO, O_2, and O_3) and their densities. We estimate their concentration in the film (discussed later) and deduce thickness of ~0.2 μm, using reported solid-state densities for CO (Roux et al. 1980), O_2 (Barrett & Meyer 1967), and O_3 (Streng & Grosse 1959). We ignore the contribution of the small amounts of residual O atoms and CO_2. These films were further capped with ~2.5 μm thick H_2O ice layer deposited at normal incidence and then heated at 1 K $minute^{-1}$ to desorption.

Specular infrared reflectance spectra of the mixed films were measured at 35° incidence using a Thermo-Nicolet Nexus 670 Fourier transform infrared spectrometer at 2 cm^{-1} resolution. The spectra were divided by the reflectance spectrum of the bare gold substrate and converted to optical depth, $-\ln(R)$. The absorption band areas of $^{13}CO_2$ and O_3 features were derived after subtraction of base lines that fit the continuum.

Using isotopic ^{13}CO (Cambridge Isotopes Labs), we were able to distinguish between $^{13}CO_2$ formed from the ^{13}CO + O reaction and adventitious $^{12}CO_2$, which condenses from thermal- or particle-induced desorption from CO_2 off the walls of the vacuum chamber or is formed by the reaction of O with adsorbed ^{12}CO. The $^{13}CO_2$ absorption is also shifted with respect to that of atmospheric $^{12}CO_2$ in the path of the infrared beam external to the vacuum system. Furthermore, we verified that any potential $^{13}CO_2$ impurity in the ^{13}CO gas was below detection limits in the infrared measurements.

3. RESULTS

Figure 2 shows the absorption features of different species in the film formed from codeposition of ^{13}CO and neutral O + O_2 at 20 K. We call this film A. From the QCM measurements, the ^{13}CO band at ~2090 cm^{-1} is due to $(273 \pm 2) \times 10^{15}$ CO cm^{-2}. The left panel shows weak bands due to absorption of solid $^{13}CO_2$ and adventitious $^{12}CO_2$. The $^{13}CO_2$ is formed from reactions between ^{13}CO and neutral O. It is weaker than the $^{12}CO_2$ band because only small quantities of $^{13}CO_2$ are formed from the $^{13}CO + O \rightarrow {}^{13}CO_2$ reaction. The right panel shows the O_3 absorption band at ~1050 cm^{-1} due to the O_2 + O reaction.

We performed a blank experiment without using O atoms: film B, also ~0.2 μm thick with a 2.5 μm ice cap, is formed by sequential deposition of known amounts of ^{13}CO (~64 ML), $^{13}CO_2$ (~0.5 ML), ^{13}CO (~195 ML), $^{13}CO_2$ (~2 ML), and O_2 (~243 ML). Both films were heated at 1 K $minute^{-1}$. Comparing the temperature dependence of CO_2 band areas in the two films (Figure 3) helps discard changes in CO_2 band area due to the interference effect (Teolis et al. 2007b). The $^{13}CO_2$ band area in film A increased by 30% during heating to 80 K. In contrast, the CO_2 band area in film B remained constant over the same temperature range, within errors. The amount of CO_2 decreased past 80 K as CO_2 leaked out of the ice cap. At ~140 K, we observed a sudden decrease in CO_2 band area as CO_2 trapped in the ice film desorbed rapidly during ice crystallization.

Similarly, we show in Figure 4 the areas of the 9.6 μm O_3 band and the 6 μm H_2O band in film A upon heating. Ozone is formed from surface reactions of O and O_2 present in the incoming flux (see the discussion). The O_3 band area remained nearly constant up to 45 K, and then doubled from 45 to 60 K. The band area then decreased between 60 and 80 K and remained nearly constant until 140 K, where it decreased sharply due to removal of trapped O_3 during ice crystallization. The fact that the 6 μm ice band barely changed when heated to 80 K indicates negligible changes in the optical properties of the film that could produce distortions due to the interference effect (Teolis et al. 2007b).

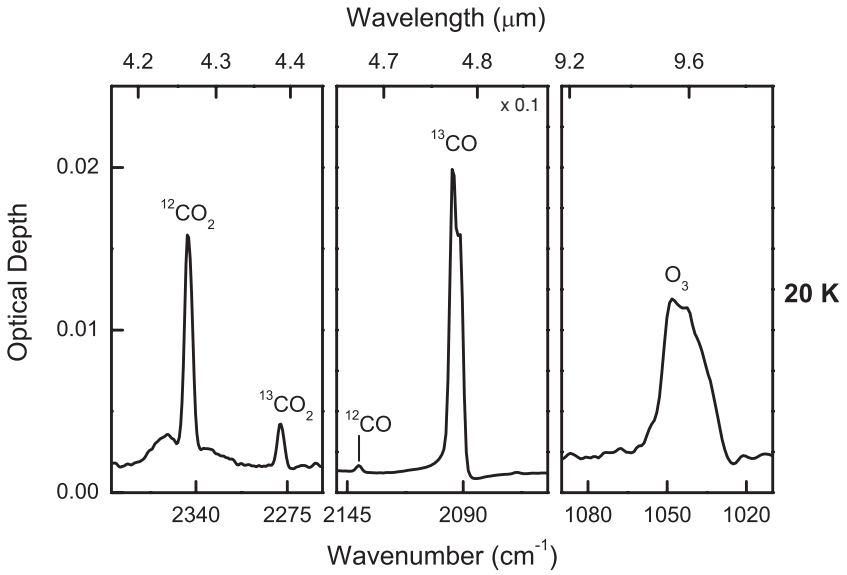

Figure 2. Infrared spectrum of the ∼0.2 μm thick film formed from codeposition of ^{13}CO and neutral O species at 20 K. ^{13}CO absorption (multiplied by 0.1) in the center panel is due to (273 ± 2) × 10^{15} CO cm^{-2}. The left and the right panels show $^{13}CO_2$ and O_3 absorption bands due to (0.3 ± 0.1) × 10^{15} CO_2 cm^{-2} and (33 ± 8) × 10^{15} O_3 cm^{-2}, respectively. $^{13}CO_2$ is formed from reactions of ^{13}CO and O, while O_3 is formed from reactions of O and O_2. The infrared spectrum also shows absorption bands due to solid ^{12}CO and $^{12}CO_2$ contaminants.

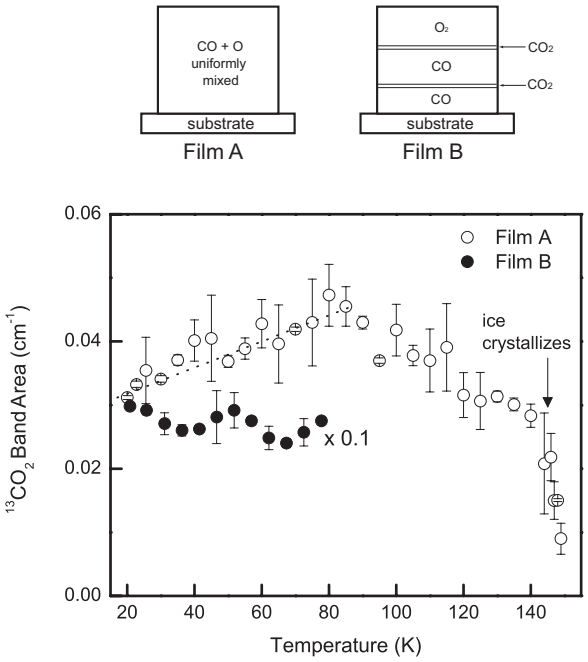

Figure 3. Evolution of the $^{13}CO_2$ absorption band area at 2280 cm^{-1} in two ∼0.2 μm thick films during heating at 1 K minute^{-1}. Film A is formed from codepositing ^{13}CO and O, O_2. Film B is formed from sequential deposition of ^{13}CO (∼64 ML), $^{13}CO_2$ (∼0.5 ML), ^{13}CO (∼195 ML), $^{13}CO_2$ (2 ML), and O_2 (243 ML). 1 ML = 1 × 10^{15} molecules cm^{-2}. Both films are capped with a 2.5 μm thick water ice film prior to heating. The 30% increase in $^{13}CO_2$ band area observed in film A and absent in film B indicates additional CO_2 from reactions between CO and residual O. The CO_2 signal decreases past 80 K since CO_2 desorbs from the ice surface. The CO_2 band area in film B is multiplied by 0.1.

4. DISCUSSION

The experiments produced CO_2 at 20 K in film A, and additionally O_3, which have not been previously observed in studies using thermal atomic beams. The presence of ozone requires that we consider that O atoms can react through three competing pathways: with CO to form CO_2, with another O to form O_2, and with O_2 to form O_3. The detection of CO_2 at 20 K contradicts a previous experiment (Roser et al. 2001) in which CO_2 was not observed after warming CO and O deposits from 5 to 60 K. This contradiction may be apparent and may have resulted from the higher signal-to-noise ratio in our experiments.

To quantify the amount of CO_2 from the infrared spectra we need the absorption band strength of CO_2. However, this band strength depends on the environment of CO_2 (mixed with other solids or segregated; Bernstein et al. 2005; Gerakines et al. 1995) and varies with film thickness in reflectance (Teolis et al. 2007b). Therefore, we cannot use the published values of band strength. Instead, we fit the reflectance spectrum of film A with a synthetic spectrum generated with Fresnel equations (Teolis et al. 2007b) that use the optical constants of the five constituents: ^{13}CO, O_2, O_3, $^{13}CO_2$, and $^{12}CO_2$. The fit, obtained by adjusting the mass fractions of five components in the film, gives 0.3 ± 0.1 ML $^{13}CO_2$ produced from the 273 ML of ^{13}CO or about 1 in 1000. We also calculate 33 ± 8 ML of ozone from its 9.6 μm absorption in Figure 2. Given the much larger production of ozone, we conclude that the majority of O atoms react either with O or O_2, rather than with CO. The reason for the low CO_2:O_3 ratio could be a small reaction barrier or strong steric effects (Braunstein & Duff 2000). The fact that the reaction O (^{3}P) + CO ($^1\Sigma^+$) → CO_2 ($^1\Sigma^+$) requires spin exchange with the lattice is probably unimportant since it may proceed through an intermediate state involving excited triplet CO_2 (Fournier et al. 1979; Braunstein & Duff 2000). We note that related experiments in warming of photolyzed mixtures of O_2 and CO diluted in solid Ar (Grim & D'Hendecourt 1986) also showed preferential formation of ozone with respect to CO_2.

We determined that the detected O_3 is formed via surface reactions between O and O_2 and is not from condensation of gas phase O_3, using a blank experiment to check the presence of gas phase O_3 in the incident flux. The bare gold substrate was exposed to the neutral beam for 30 minutes at 50 K, where only O_3 can condense. The substrate was further cooled to 20 K and again exposed to the atom source for an additional 30 minutes, where both O and O_2 can condense. The mass uptake rate at 50 K was 5% of that at 20 K; infrared spectroscopy determined

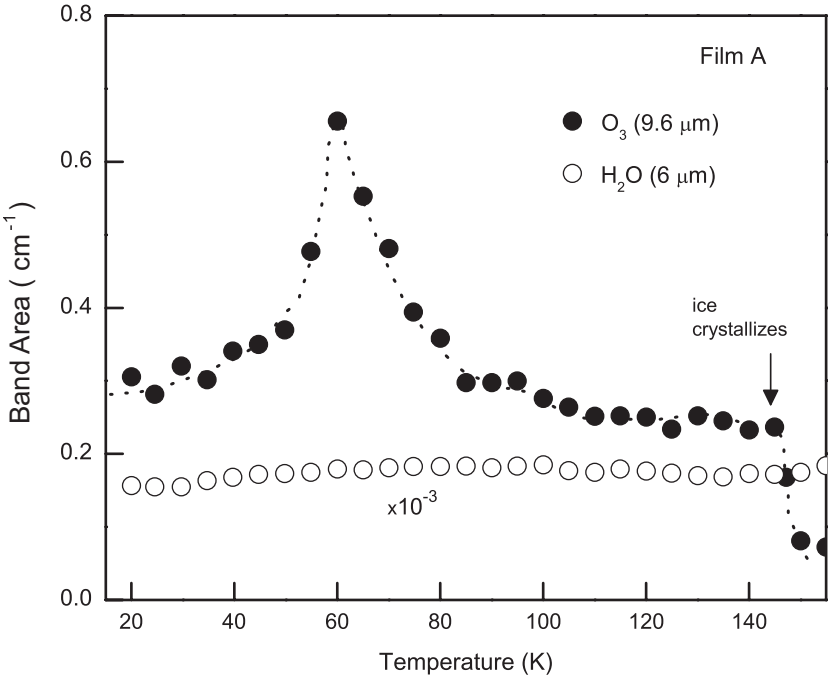

Figure 4. Evolution of the band areas of the 9.6 μm O_3 and 6 μm H_2O absorptions in film A during heating at 1 K minute^{-1}. The O_3 band area doubles between 45 and 60 K, where ozone crystallizes. Past 60 K, O_3 diffuses out of ice leading to a decrease in the band area. The 6 μm H_2O band area remains nearly constant up to ~140 K where ice crystallizes, releasing the remaining ozone. The band area of 6 μm absorption is multiplied by 10^{-3}.

that this uptake was due to background water and not ozone. However, O_3 formed during the second 30-minute exposure at 20 K, as indicated by the presence of the 9.6 μm infrared band.

The 30% increase in $^{13}CO_2$ band area during warm-up in film A (Figure 3) suggests that thermal diffusion of unreacted O atoms and ^{13}CO molecules induced further reactions to form additional $^{13}CO_2$. The water ice cap traps the CO and O species in the ice nanopores (Raut et al. 2007) to temperatures higher than those at which surface CO sublimes rapidly.

The ozone band area in film A remained nearly constant when heated up to 45 K and then increased rapidly up to 60 K (Figure 4). This behavior is possibly due to residual O that reacts with O_2 to form additional O_3. However, the fast rise in the signal is more likely related to the sharp increase in the absorption strength of ozone due to crystallization between 47 and 53 K (Teolis et al. 2007a). The O_3 signal drops above 60 K due to diffusion to the surface, from where it can desorb thermally. The 6 μm H_2O band area remains nearly constant up to 80 K, showing that the change in the O_3 band area is not an optical interference effect.

5. ASTROPHYSICAL IMPLICATION

Abundant CO has also been detected in both gas and solid phase, with 10–100 times more CO in the gas phase (van Dishoeck et al. 1996). The existence of gas phase oxygen is inferred from comparison between the expected O abundance and the oxygen tied up in solid and gaseous O_2, CO, CO_2, and H_2O. It has been suggested that a fraction of the missing oxygen exists as atomic O in dark molecular clouds (Vandenbussche et al. 1999) with O abundance comparable to that of CO gas. It has been estimated that the CO molecules strike a grain once every few days (Tielens 2005). Formation of CO_2 can occur on the grains when CO and O atoms accrete from the gas phase in close proximity, diffuse and react, or CO_2 can form directly when an incoming O collides with a surface CO. The observation of direct CO_2 formation at 20 K on laboratory timescales shows that this synthesis mechanism can indeed contribute to the observed CO_2 over the lifetime of the molecular clouds (~10^7 yr) and, additionally, that it can occur in dark clouds where the ultraviolet flux is small, ~10^3–10^4 photons cm^{-2} s^{-1} (Prasad & Tarafdar 1983). Other formation mechanisms that do not require radiation are suggested by recent experiments showing that CO_2 forms when solid CO is exposed to products of a water discharge (Oba et al. 2010) and when mixed films of CO and O_2 are exposed to H atoms (Ioppolo et al. 2011).

O atoms are reactive radicals and can react with molecules other than CO. Our experiments show that, in the presence of O_2, formation of ozone is favored over CO_2, which is also found in matrix-isolation studies (Grim & D'Hendecourt 1986). This suggests that there may exist other sinks for O, such as in-grain reactions with abundant H and H_2. The competition for O would depend on the relative concentration of different species that can potentially react with O and the size of any reaction barrier.

Although the measured CO_2:CO ratio of 0.001 is at least 100 times smaller than that observed in interstellar ice mantles (Cook et al. 2011), there are many phenomena that can significantly enhance the ratio after synthesis. Both thermal desorption and particle-induced desorption/sputtering preferentially remove the more volatile CO. Preferential CO desorption can occur during transient heating in grain–grain collisions or by an impact of an energetic particle such as a cosmic ray.

The formation of ozone, an important observation in this work, is difficult to put in an interstellar context since the abundance of O and O_2 is still an unsolved problem (Hollenbach et al. 2009; Jenkins 2009; Whittet 2010). The lack of positive detection of solid ozone in molecular clouds is not conclusive since the strong broad silicate band absorption at 10 μm can easily mask the 9.6 μm ozone feature. In favorable cases, weak structures can be seen in the 8.5–10 μm region. Recent spectra toward *IC 5146* (Chiar et al. 2011) is compatible with

the presence of NH_3, O_3, and CH_3OH but does not allow unambiguous identification. The presence of ozone on dust grains presents interesting additional possibilities. Due to its low bond energy (1.1 eV), ozone would easily be photodissociated to produce hot O atoms that could react locally with CO and produce CO_2 (Madzunkov et al. 2006).

We acknowledge the support from NSF Astronomy and NASA Origins programs. We thank Dr. Ben Teolis (SWRI) for insightful discussions and Emma Mitchell for her critical reading of the manuscript.

REFERENCES

Barrett, C. S., & Meyer, L. 1967, Phys. Rev., 160, 694
Bernstein, M. P., Cruikshank, D. P., & Sandford, S. A. 2005, Icarus, 179, 527
Boogert, A. C. A., Ehrenfreund, P., Clayton, G. C., & Draine, B. T. 2004, in ASP Conf. Ser. 309, Astrophysics of Dust, ed. A. N. Witt, G. C. Clayton, & B. T. Draine (San Francisco, CA: ASP), 547
Braunstein, M., & Duff, J. W. 2000, J. Chem. Phys., 112, 2736
Chiar, J. E., Pendleton, Y. J., Allamandola, L. J., et al. 2011, ApJ, 731, 9
Cook, A. M., Whittet, D. C. B., Shenoy, S. S., et al. 2011, ApJ, 730, 124
Fournier, J., Deson, J., Vermeil, C., & Pimentel, G. C. 1979, J. Chem. Phys., 70, 5726
Gerakines, P. A., & Moore, M. H. 2001, Icarus, 154, 372
Gerakines, P. A., Schutte, W. A., Greenberg, J. M., & van Dishoeck, E. F. 1995, A&A, 296, 810
Grim, R. J. A., & D'Hendecourt, L. B. 1986, A&A, 167, 161
Hollenbach, D., Kaufman, M. J., Bergin, E. A., & Melnick, G. J. 2009, ApJ, 690, 1497
Ioppolo, S., van Boheemen, Y., Cuppen, H. M., van Dishoeck, E. F., & Linnartz, H. 2011, MNRAS, 413, 2281
Jenkins, E. B. 2009, ApJ, 700, 1299
Loeffler, M. J., Baratta, G. A., Palumbo, M. E., Strazzulla, G., & Baragiola, R. A. 2005, A&A, 435, 587
Madzunkov, S., Shortt, B. J., Macaskill, J. A., Darrach, M. R., & Chutjian, A. 2006, Phys. Rev. A, 73, 20901
Mulcahy, M. F. R., & Williams, D. J. 1968, Trans. Faraday Soc., 64, 59
Noxon, J. F. 1970, J. Chem. Phys., 52, 1852
Oba, Y., Watanabe, N., Kouchi, A., Hama, T., & Pirronello, V. 2010, ApJ, 712, L174
Prasad, S. S., & Tarafdar, S. P. 1983, ApJ, 267, 603
Raut, U., Fama, M., Teolis, B. D., & Baragiola, R. A. 2007, J. Chem. Phys., 127, 204713
Roser, J. E., Vidali, G., Manicò, G., & Pirronello, V. 2001, ApJ, 555, L61
Roux, J. A., Wood, B. E., Smith, A. M., & Plyler, R. R. 1980, Infrared Optical Properties of Thin CO, NO, CH_4, HCl, N_2O, O_2, N_2 Ar, and Air Cryofilms, Report AEDC-TR-79-81 (DTIC Accession No. AD-A088269), 12
Sack, N. J., & Baragiola, R. A. 1993, Phys. Rev. B, 48, 9973
Satorre, M. A., Palumbo, M. E., & Strazzulla, G. 2000, Ap&SS, 274, 643
Sethi, D. S., & Smith, A. L. 1975, Planet. Space Sci., 23, 661
Sharpe, S., Boiani, J. A., & Sethi, D. S. 1988, Int. J. Chem. Kinetics, 20, 967
Slanger, T. G. 1972, J. Chem. Phys., 57, 233
Streng, A. G., & Grosse, A. V. 1959, J. Am. Chem. Soc., 81, 805
Teolis, B. D., Fama, M., & Baragiola, R. A. 2007a, J. Chem. Phys., 127, 074507
Teolis, B. D., Loeffler, M. J., Raut, U., Famá, M., & Baragiola, R. A. 2007b, Icarus, 190, 274
Tielens, A. G. G. M. 2005, The Physics and Chemistry of the Interstellar Medium (Cambridge: Cambridge Univ. Press)
Vandenbussche, B., Ehrenfreund, P., Boogert, A. C. A., et al. 1999, A&A, 346, L57
van Dishoeck, E. F., Helmich, F. P., de Graauw, T., et al. 1996, A&A, 315, L349
Watanabe, N., & Kouchi, A. 2002, ApJ, 567, 651
Welge, K. H., & Atkinson, R. 1976, J. Chem. Phys., 64, 531
Whittet, D. C. B. 2010, ApJ, 710, 1009